THE JOURNAL OF PHYSICAL CHEMISTRY C
A JOURNAL OF THE AMERICAN CHEMICAL SOCIETY

pubs.acs.org/JPCC
Article

Unveiling Reaction Pathways of Ethylene Carbonate and Vinylene Carbonate in Li-Ion Batteries

Robin Lundström,* Neeha Gogoi, Tim Melin, and Erik J. Berg*

Cite This: J. Phys. Chem. C 2024, 128, 8147−8153
Read Online

ACCESS | Metrics & More | Article Recommendations | Supporting Information

ABSTRACT: Ethylene carbonate (EC) and vinylene carbonate (VC) are the archetypical electrolyte solvent and additive in Li-ion batteries (LIBs), respectively. However, our understanding of their reaction pathways remains incomplete. Herein, the reaction pathways of EC and VC are explored by using online electrochemical mass spectrometry complemented by nuclear magnetic resonance analysis. For EC, reduction occurs through two distinct pathways <0.8 V vs Li^+/Li, one yielding C_2H_4 and the other yielding CO, depending on the electrode potential and the EC concentration. The CO-releasing pathway does not contribute to the solid electrolyte interphase formation. For VC, reduction commences at <1.9 V, but CO_2 gas evolution proceeds through a chemical step via a nucleophilic attack and VC ring opening. Additionally, VC scavenges H_2O and reduced protons via hydrolysis and via proton abstraction from the carbon electrode to form EC. Our study uncovers further reaction pathways and underscores the unique properties of EC and VC, both individually and in combination, and elucidates their roles in influencing the formation process in Li-ion batteries.

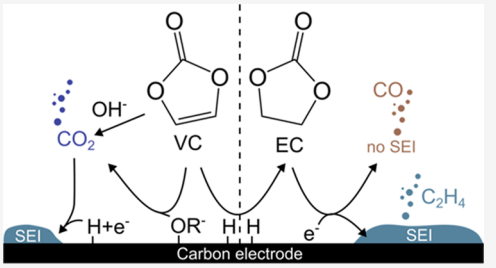

INTRODUCTION

Despite the widespread application of Li-ion batteries (LIBs) today, there are still essential aspects of this energy storage technology that are not fully understood. Particularly, the solid electrolyte interphase (SEI) on the graphite negative electrode remains elusive.[1] The formation of the SEI primarily proceeds through electrochemical reduction reactions of the electrolyte and its additives, a process that is well known to be critical for LIB performance and lifetime. Multiple SEI reaction pathways have been proposed and most of them are still debated.[2] Since several reactions trigger gas evolution, careful analysis thereof, as with online electrochemical mass spectrometry (OEMS), has turned out as one of the most powerful approaches to investigate SEI reactions.[3,4]

Ethylene carbonate (EC) is the most commonly used LIB electrolyte solvent, largely because it forms an SEI on the negative electrode when reduced at potentials <0.8 V vs Li^+/Li. Several EC reduction reaction pathways have been proposed (Scheme 1),[2,5−7] where lithium ethylene dicarbonate (LEDC) and Li_2CO_3 are commonly reported as the main products along with the release of gaseous C_2H_4.[8−11] The process behind Li_2CO_3 formation is still under debate.[12,13] While C_2H_4 is the predominantly observed gas, EC reduction is also reported to generate CO along with (Li^+/poly) ethylene glycol [(Li/P)EG] and their derivatives.[5,7,14] However, which factors favor which EC reduction reaction pathway is still unknown.

While EC is the most well-known LIB solvent, vinylene carbonate (VC) is the likewise electrolyte additive.[15] Both the anode[16,17] and cathode[18,19] are affected by VC, although a positive effect is mainly observed at the anode. VC is commonly reported to form an SEI before EC (>1.0 V vs Li^+/Li),[16] even though the exact potential onset for the reaction is still undetermined (reported potentials range from 2.0 to 1.0 V vs Li^+/Li).[16,20−23] A VC-derived SEI is commonly reported to consist primarily of poly(VC) (e.g., via Scheme 2 as suggested by Zhang et al.[20]) together with other linear oligomeric/polymeric compounds, as observed by infrared

Scheme 1. Few Commonly Reported EC Reduction Reaction Pathways

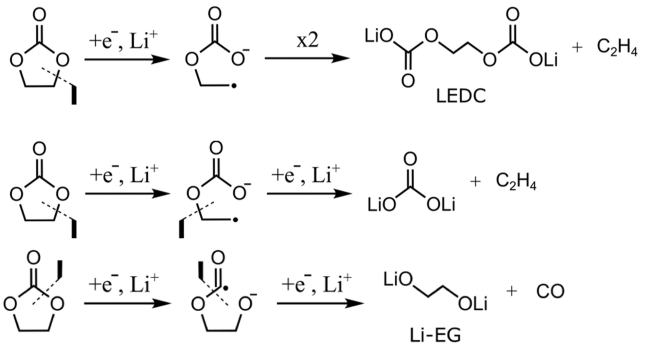

Received: February 12, 2024
Revised: April 29, 2024
Accepted: April 29, 2024
Published: May 9, 2024

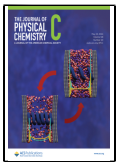

https://doi.org/10.1021/acs.jpcc.4c00927
J. Phys. Chem. C 2024, 128, 8147−8153

Scheme 2. Possible VC Reduction Reaction Pathway Forming Poly(VC)

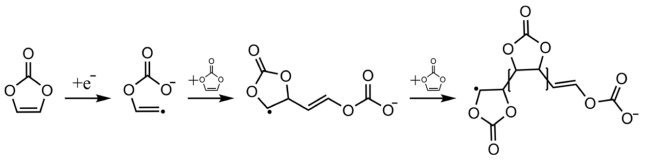

(IR),[16,22−26] nuclear magnetic resonance (NMR),[16,22−24] X-ray photoelectron spectroscopy (XPS),[22,27] and transmission electron microscopy (TEM)[22,26] studies. Despite the numerous reports and the major impact of VC on the LIB industry, a clear understanding of VC reaction pathways is lacking, and open questions still remain. For instance, why is not poly(VC) always reported?[28] Why is there strong CO_2 evolution observed during VC reduction,[20,21,25] which in turn should be unrelated to poly(VC) formation?

Herein, we elucidate further EC and VC reaction pathways by applying a simplified model electrode/electrolyte system. The study aims to add more pieces to the SEI puzzle toward complete understanding of the SEI in modern LIBs.

METHODS

Glassy carbon (GC) electrodes were prepared as a slurry by mixing 95 wt % GC powder (Sigma-Aldrich, spherical powder, 2−12 μm, 99.95% trace metals basis, A_{BET} = 1.8 $m^2\ g^{-1}$) and 5 wt % PVDF (polyvinylidene fluoride, Kynar HSV 900, Arkema) dissolved in NMP solvent (Sigma-Aldrich). The slurry was mixed with a Polytron PT 2500 E mixer (KINEMATICA GmbH, Germany) until a homogeneous slurry was achieved. The slurry was coated onto a stainless-steel mesh (212/90 μm, Bopp AG, Switzerland) using a 150 μm doctor blade. After coating, the electrodes were dried at room temperature and punched into 14 mm disks, before being further dried at 120 °C under vacuum for 12 h.

The electrolytes used in all experiments consisted of 0.2 M $LiClO_4$ (battery grade >99.99%, Sigma-Aldrich) in 1,2-dimethoxyethane (DME, 99.9%, Honeywell) as a base. The desired concentrations of VC (99.5%, Sigma-Aldrich) and EC (>99%, Sigma-Aldrich) were added to the base electrolyte. A single Celgard 2325 separator (dried for 6 h at 70 °C in a vacuum) was used for all cells.

The commercial $LiFePO_4$ (LFP) electrodes (1 mAh cm^{-2}, Customcells) were punched into 15 mm disks and dried at 120 °C under vacuum for 12 h. The LFP electrodes were electrochemically delithiated to ∼90% state of charge (SOC) in LFP | 0.2 M $LiClO_4$ DME | Li cells to achieve a stable potential plateau (herein assumed to be 3.43 V vs Li^+/Li) before any experiment (same procedure as described in our earlier study[29]). All potentials presented from this point onward are vs Li^+/Li.

For online electrochemical mass spectrometry (OEMS), all cells were assembled in an electrode sandwich configuration, comprising GC | 150 μL of 0.2 M $LiClO_4$ DME:VC:EC | LFP (90% SOC). The cycling protocol was 5 h open-circuit voltage (OCV) followed by cyclic voltammetry (CV) from OCV (∼3.1 V) with vertex potentials of 0.5 and 1.7 V. The scan rate was 0.1 mV/s. The experiments were conducted at 30 °C, and the gas was purged and analyzed every 10 min. The MS was calibrated with H_2, CH_4, C_2H_4, and CO, O_2, and CO_2 calibration gases. A detailed description of the OEMS system is found in our earlier study.[30]

For nuclear magnetic resonance (NMR) cells, constant current was applied to a GC | 400 μL of 0.2 M $LiClO_4$ DME (or DMSO):VC:EC (0 or 10 v%: 0 or 10 v%) | LFP (90% SOC) system, until 0.5 V was reached, where the potential was held for 3 h. Thereafter, the electrolyte was extracted to NMR tubes. The cycled cells with EC, VC, and EC:VC-added electrolytes were used for NMR analysis, and deuterated DMSO-d_6 was used as the background solvent. All spectra were recorded at room temperature, and anhydrous DMSO-d_6 was used as the internal standard for ^1H and ^{13}C NMR. All NMR spectra were obtained using a Bruker 3 channel cryoprobe NMR spectrometer (600 MHz (^1H), 162 MHz (^{13}C)). The conditions for the ^1H NMR were 45° pulse angle, 8 s delay between pluses, 20.0 kHz spectral width, and 64 scans. The conditions for the ^{13}C NMR were 45° pulse angle, 1.8 s delay between pluses, 27 kHz spectral width, and 1024 scans.

RESULTS AND DISCUSSION

Figure 1 shows the cyclic voltammogram and associated gas evolution data of C_2H_4 and CO for the model GC | 0.2 M $LiClO_4$ DME:EC | LFP (90% SOC) cells containing EC in the range of n_{EC} = 0−1560 $nmol_{EC}\ cm_{GC}^{-2}$. All data are normalized to the GC electrode surface area (A_{GC}). A GC-based electrode was applied to study electrolyte reduction on carbon and avoid effects associated with solvent cointercalation into graphite. Furthermore, in order to reduce the interference of the solvent and salt, DME and $LiClO_4$ are employed. DME was chosen as a base electrolyte solvent due to its low reduction potential[31] and the high achievable purity to minimize residual contaminants. $LiClO_4$ was chosen over the commercially used $LiPF_6$, as the latter is known to be reactive toward electrolyte reduction products,[32] which would add further complexity to the system.

Figure 1a shows the cyclic voltammogram of the first cycle, revealing consistent current profiles across all of the EC-containing cells. A distinct current peak at 1.6 V, attributed to the reduction of H_2O impurities, marks the first noticeable electrochemical reaction. As the potential drops <1.2 V, there is an increase in current, primarily due to the reversible adsorption of Li^+.[33] Below 0.8 V, currents corresponding to the reduction of EC emerge. Notably, as n_{EC} increases in the cells, the reversible charge decreases, which apart from lithium loss also suggests an increased cell resistance with higher n_{EC}.

C_2H_4 evolves <0.8 V as expected for cells with n_{EC} > 0 $nmol_{EC}\ cm_{GC}^{-2}$ in the electrolyte. The registered total C_2H_4 amounts reach an upper limit of ∼3 nmol $C_2H_4\ cm_{GC}^{-2}$ for cells with $n_{EC} \geq 80\ nmol_{EC}\ cm_{GC}^{-2}$ (Figure 1b,d), which means that a similar number of mols of EC are needed to passivate the GC surface, according to Scheme 1. The amounts of C_2H_4 drop off <80 $nmol_{EC}\ cm_{GC}^{-2}$, indicating that n_{EC} is lower than needed for a fully passivating SEI, which is also evident from the second cycle where additional C_2H_4 evolution is detected in the dilute EC cells (Figure S1). The C_2H_4 onset shifts from ∼0.5 to >0.7 V as n_{EC} increases, which is attributed to at least two factors: a concentration-dependent EC reaction pathway and limited mass transport of EC to the electrode surface at lower n_{EC}. Although the LEDC or Li_2CO_3 reaction pathways (Scheme 1) are indistinguishable here, the strongly shifting C_2H_4 potential onset indicates that the more concentration-dependent LEDC formation pathway (2 EC/C_2H_4 compared to Li_2CO_3 formation pathways) is likely the governing SEI process. Evidence of competing EC reaction pathways is found in analysis of the concomitant CO evolution (Figure 1c). Unlike

https://doi.org/10.1021/acs.jpcc.4c00927
J. Phys. Chem. C 2024, 128, 8147−8153

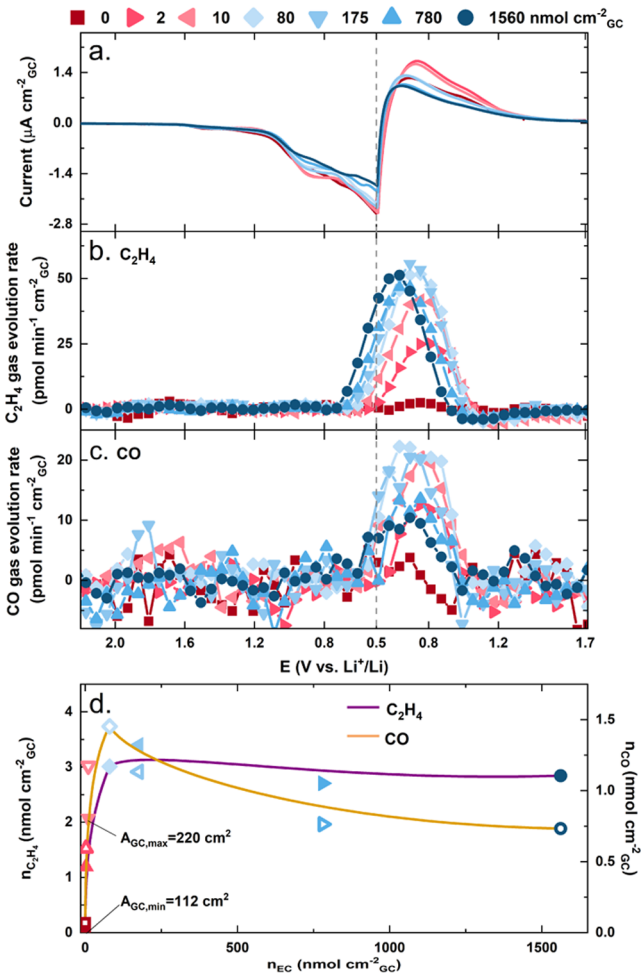

Figure 1. OEMS data for GC | 0.2 M $LiClO_4$ DME:EC | LFP (90% SOC) cells with different n_{EC} cycled with CV at 0.1 mV/s rate. The gray vertical dashed line represents the vertex potential 0.5 V. The legend shows n_{EC} in every cell. (a) Current profiles for the initial cycle. (b) C_2H_4 gas evolution trend from EC reduction in the initial cycle. (c) The CO gas evolution trend from EC reduction in the initial cycle. (d) Total C_2H_4 and CO evolution for different n_{EC}. The maximum and minimum GC surface areas are labeled for the experiment series. The markers are closed for C_2H_4 and open for CO.

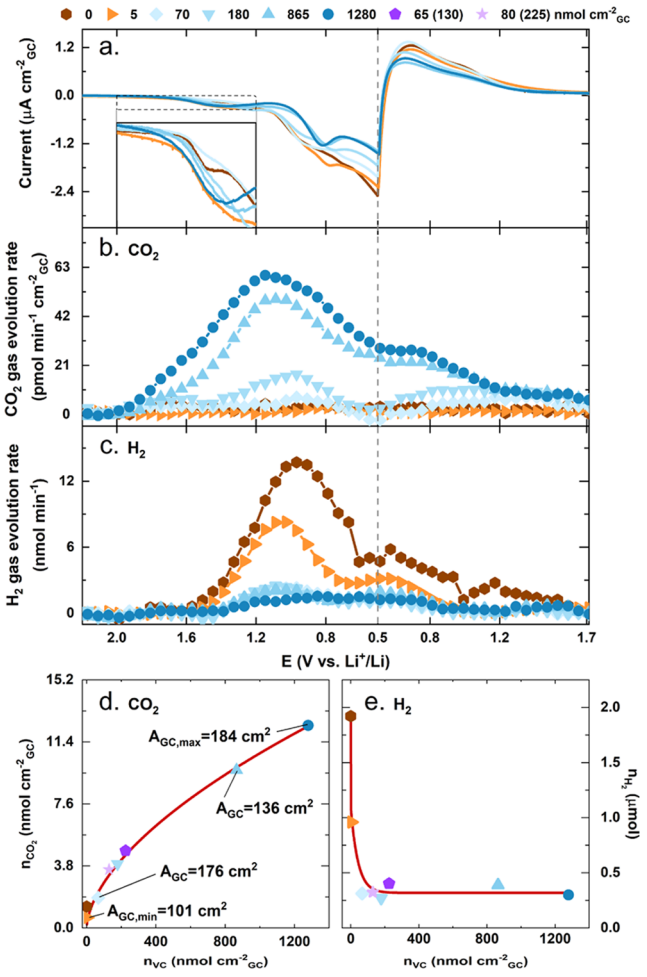

Figure 2. OEMS data for a GC | 0.2 M $LiClO_4$ DME:VC | LFP (90% SOC) system cycled with CV at 0.1 mV/s rate. The gray vertical dashed line represents the vertex potential of 0.5 V. The legend shows n_{VC} in every cell. (a) Electrochemical profiles for the different cells during the initial cycle, with a zoom-in on the >1.2 V electrochemical profiles. (b) CO_2 gas evolution trend from VC in the initial cycle. (c) H_2 gas evolution trend in the initial cycle. (d) Total CO_2 evolution for different n_{VC}. A_{GC} is labeled for selected cells (full list in Table S1). (e) Total H_2 evolution for different n_{VC}. The cells denoted 65 (130) and 80 (225) are a mix of VC and EC (only shown in (d) and (e)), where the first value is n_{VC} and the value in parentheses is n_{VC+EC}.

C_2H_4, the CO gas evolution always sets in at ~0.6 V regardless of n_{EC} and the total amount of CO displays a different trend compared to C_2H_4 (Figure 1d), thus indicating that the processes behind the evolution of these two gases follow different kinetics. For instance, the cells with ~3 nmol C_2H_4 cm_{GC}^{-2} (colored blue in Figure 1) evolution show an increase in CO evolution as n_{EC} decreases, which demonstrates that the EC reduction pathways are n_{EC}-dependent. However, the CO-evolving EC reaction pathway, with lithium Li-glycol (Li-EG) as a product (Scheme 1), does likely not contribute to the SEI as ~3 nmol C_2H_4 cm_{GC}^{-2} is still detected, i.e., the SEI formation process would be less efficient at lower n_{EC}.

H_2 gas evolution was observed in all cells, as shown in Figure S1. The presence of EC in the electrolyte consistently suppressed a portion of the H_2 evolution, even though a definitive trend was not evident.

Figure 2 shows the cyclic voltammogram and gas evolution trends of CO_2 and H_2 for GC | 0.2 M $LiClO_4$ DME:VC:EC | LFP (90% SOC) cells with electrolyte mixtures of VC (n_{VC} = 0−1280 $nmol_{VC}$ cm_{GC}^{-2}) mixed with EC (n_{EC} = 0−145 $nmol_{EC}$ cm_{GC}^{-2}). The first observable electrochemical reaction is distinguishable in the range of 1.9−1.6 V in the current profile (Figure 2a). All VC-containing cells have a similar negative current slope down to ~1.4 V without a clear H_2O reduction plateau compared to that of the pure DME cell. The two highest n_{VC} cells (≥865 $nmol_{VC}$ cm_{GC}^{-2}) reach a current peak at 1.4−1.3 V, indicating an early fully covering SEI layer, which does not develop to the same extent in the ≤180 $nmol_{VC}$ cm_{GC}^{-2} cells, as seen in the inset of Figure 2a. A new current peak is observed at ~0.8 V for the VC-containing cells with ≥865 $nmol_{VC}$ cm_{GC}^{-2} and is related to CO_2 consumption <1.0 V as discussed below.[25,29] Similar current intensity profiles are present for lower n_{VC} cells too but to a lesser extent. A general trend of lower reversible charge per A_{GC} with increasing n_{VC} is observed, as seen in Figure S4. Indeed, the SEI layer formed by VC has previously been reported to increase the internal resistance of Li-ion cells, which explains such a trend.[21,34,35] A

https://doi.org/10.1021/acs.jpcc.4c00927
J. Phys. Chem. C 2024, 128, 8147−8153

less efficient Li-adsorption process as a result of the buildup of the VC-based SEI can, however, not be ruled out.

CO_2 gas evolution is detected already >2.0 V before the current onset at ∼1.9 V for the cell with the highest n_{VC} of 1280 $nmol_{VC}$ cm_{GC}^{-2}. However, CO_2 gas evolution is shifted to lower potentials and decreased gas evolution rates are detected with lesser n_{VC} until no CO_2 is present in the pure DME cell (Figure 2b). CO_2 has previously been suggested to originate from an initial electrochemical reduction process of VC along with a chemical propagation step.[20] However, we hypothesize that CO_2 from VC at these potentials rather stems from VC ring opening via a nucleophilic attack by reduced surface oxygens on the carbon electrode, which are generated at potentials <2.6 V,[29] as virtually no reduction current is detected at this stage—an observation that agrees with the study by Schwenke et al.[25] A CO_2 consumption reaction is present <1.0 V and is seen as an indent in the gas evolution rate, resulting in a decline in gas evolution rate in all VC-containing cells. The first CO_2 consumption reactions are associated with the parallel consumption of surface hydrogens as a similar indent in the gas rate profile is present in the H_2 gas evolution data in Figure 2c, likely forming lithium formate (HCO_2Li, Scheme 3) as discussed below.

Scheme 3. Lithium Formate Formation

$$Li^+ + CO_2 + H^+ + 2e^- \rightarrow HCO_2Li$$

The volume of the evolved CO_2 gas in the initial cycle increases with increasing n_{VC} (Figure 2d), in agreement with the study by Petibon et al.[36] The amount of CO_2 evolved scales virtually with the square root of n_{VC} as could be expected if the rate of evolution of CO_2 in VC-containing cells is controlled by the distance between VC molecules. No clear evidence regarding how much VC is reacting can be garnered from the OEMS data. However, as the total amount of CO_2 evolved is much lesser than the amount of VC present, it can be assumed that reaction pathways where no CO_2 is released take place, e.g., via the formation of different oligomers/polymers where the carbonate groups may be intact. Such pathways have been reported in the literature[16,23,24] and will be discussed later herein.

H_2 evolution onsets at ∼1.6 V in all EC-containing cells (Figure S1), the pure DME cell, and the cell containing 5 $nmol_{VC}$ cm_{GC}^{-2} (Figure 2c). All other VC-containing cells have the H_2 gas evolution significantly suppressed at ∼1.6 V. Two distinct H_2 evolution peaks are observed, the first reaching its maximum at ∼1.0 V with the second at ∼0.5 V (Figure 2c). The presence of two peaks is likely attributed to the formation of HCO_2Li at around 1.0 V (Scheme 1), which causes a decrease in the gas evolution rate. This suggests a single main H_2 evolving process rather than two distinct H_2-evolving reactions, which agrees with the study by Metzger et al. where H_2 evolution was reported to mainly originate from H_2O reduction.[37] The H_2 gas evolution rate is not normalized to the surface area but is reported as the absolute value since H_2O is expected to be found throughout the cell and not contributing significantly to the SEI on the GC. The formation of a VC-based blocking layer has been suggested as the reason for the lowered H_2 evolution.[38] However, we hypothesize that VC when ring-opened (and releasing CO_2) scavenges H_2O, which would as a result be the reason for decreased mols of evolved H_2. Notably, irrespective of the n_{VC}, the H_2 evolution was never completely suppressed. Instead, a plateau of 0.3 μmol H_2 is reached at 70 $nmol_{VC}$ cm_{GC}^{-2} and is not affected by higher n_{VC}. Therefore, another H_2 source other than H_2O reduction is likely present, where surface groups on the carbon are possible candidates.

Another observation is that cells containing VC as the sole cyclic carbonate noticeably evolve CO_2 and cells containing EC as the sole cyclic carbonate show no clear sign of CO_2 evolution (Figure S3). However, a similar amount of CO_2 evolves in cells where VC and EC are mixed together (Figures 2d and S3) as for cells containing only VC, if the CO_2 gas evolution is normalized to the total number of mols of cyclic carbonates in the cells, i.e., n_{VC+EC}. In other words, the VC reaction pathway releasing CO_2 does not discriminate between EC and VC during the propagation step (Figure 4), and ring-opened VC apparently can react with EC in the electrolyte. Notably, mixing EC and VC does not alter the trend of H_2 gas evolution (Figure 2e) as the same plateau of 0.3 μmol is reached for the mixed EC:VC cells as for the VC-only cells.

The products from EC and VC reactions were further investigated by NMR as shown in Figure 3. No clear evidence

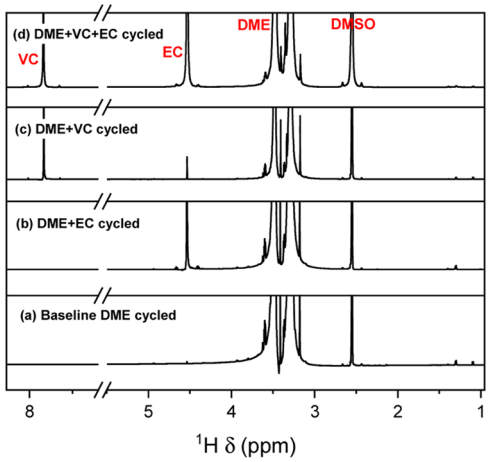

Figure 3. NMR data of GC | 0.2 M $LiClO_4$ DME:VC:EC | LFP (90% SOC) cells cycled at constant current until 0.5 V and held at the potential for 3 h. The electrolytes used were (a) 0.2 M $LiClO_4$ DME, (b) 0.2 M $LiClO_4$ DME + 10 v% EC, (c) 0.2 M $LiClO_4$ DME + 10 v % VC, and (d) 0.2 M $LiClO_4$ DME + 10 v% EC + 10 v% VC.

of soluble reduction products was detected in EC, VC, or EC:VC cells. However, the cell containing only VC (∼1.6 M) before cycling contains 3 mM EC after cycling. A similar effect was detected with OEMS (Figure S2), where C_2H_4 was detected in cells at low n_{VC} even though no EC (n_{EC} = 0) was added. We therefore propose that VC can abstract reduced protons from the GC surface and turn into EC. The reason for only detecting C_2H_4 at low n_{VC} in the OEMS is due to the VC-derived SEI not fully covering the GC surface, and the EC thus formed can be reduced at the uncovered GC surface to the extent at which it is detectable.

Next, the DME electrolyte was exchanged for DMSO-d_6 during cycling in an attempt to identify possible SEI products (Figure S6). The GC | 0.2 M $LiClO_4$ DMSO:VC:EC (0 or 10 v%: 0 or 10 v%) | LFP (90% SOC) cells were cycled to 1.0 V, and the potential was held for 3 h before the electrolyte was extracted for NMR analysis. Lithium formate was detected, which agreed with the OEMS conclusions. Additionally, vinoxyl groups (CH(=O)−CH_2R) are present along with a

https://doi.org/10.1021/acs.jpcc.4c00927
J. Phys. Chem. C 2024, 128, 8147−8153

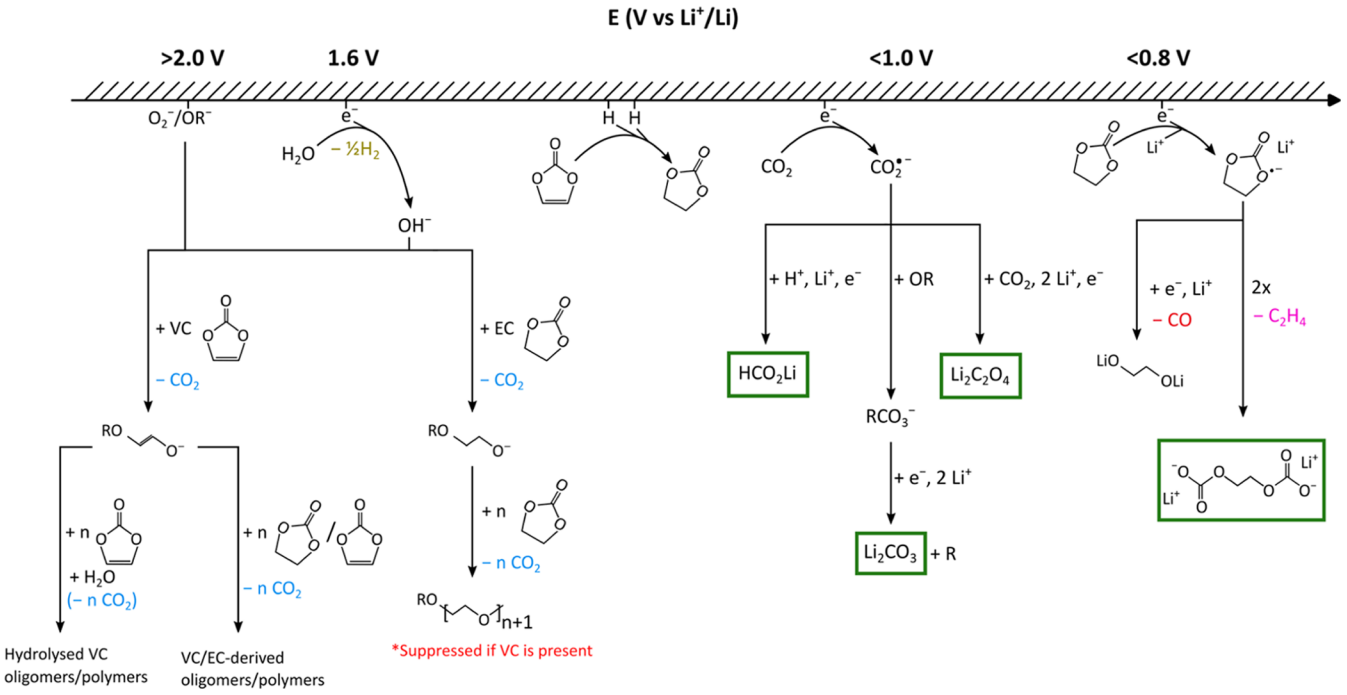

Figure 4. Schematic of suggested VC and EC reaction pathways on a carbon electrode based on the findings in this study and literature.[9,25,29] The top potential axis represents the potential at the GC. Gaseous products are colored (CO_2 is blue, H_2 is dark yellow, C_2H_4 is pink, and CO is red). Boxed-in products are solid/SEI products. Further end products dissolve in the electrolyte and do not contribute to the SEI.

range of VC-derived polymers. Notably, PEG forms in the EC-only cell but is completely suppressed if VC is also included, hence demonstrating that VC suppresses EC hydrolysis and the subsequent formation of PEG.

CONCLUSIONS

The reduction reaction pathways of EC and VC on carbon have been investigated by *operando* gas analysis, and our conclusions are schematically illustrated in Figure 4. First, EC reduction follows two distinct reduction pathways, one releasing C_2H_4 and the other releasing CO. The extent to which each reaction pathway occurs is governed by electrode potential and EC concentration. While the C_2H_4-evolving pathway contributes to the SEI, likely by forming LEDC, the CO-evolving pathway does not. Second, CO_2 generated from VC does not originate from VC reduction but from a ring opening process. Third, VC efficiently suppresses H_2 evolution by scavenging reduced protons in two distinct processes. Rather than forming a blocking SEI layer restricting access for H_2O to the reductive carbon surface, VC supports the consumption of reduced protons on the surface by forming EC and generating CO_2, which, in turn, scavenges protons to form Li-formate. Fourth, regardless of n_{VC}, a constant H_2 gas evolution plateau is reached, indicating that different H_2 sources from H_2O are present in the cells. We hypothesize that they are protic surface groups, which cannot be scavenged by VC. Fifth, the species formed from EC and VC reduction and decomposition reactions differ significantly, with different oligomers/polymers forming. Sixth, by mixing EC and VC, the resulting products are more similar to products in the VC-only cells compared to the EC-only cells, hence indicating that VC governs the SEI formation process when present. Finally, the reaction pathways of EC and VC are further complicated when both cyclic carbonates are present, as their reaction pathways are intertwined.

Our results deepen the understanding of the SEI formation reactions involving VC and EC. The processes identified herein are easily overlooked and challenging to identify in a commercial battery cell environment where multiple reactions overlap and overshadow these processes, thus showcasing the importance of studying model systems to understand and model the SEI in LIBs.

ASSOCIATED CONTENT

Supporting Information

The Supporting Information is available free of charge at https://pubs.acs.org/doi/10.1021/acs.jpcc.4c00927.

Online electrochemical mass spectrometry data of GC | 0.2 M $LiClO_4$ DME:EC | LFP, GC | 0.2 M $LiClO_4$ DME:VC | LFP, and GC | 0.2 M $LiClO_4$ DME:EC:VC | LFP cells, generated charge during CV sweeps for EC- and VC-containing cells, calculations to determine the H_2O content in cells and tabulated values comparing the H_2O content to the VC content in VC-containing cells, extended NMR data of DME-based electrolytes, and NMR data of DMSO-based electrolytes (PDF)

AUTHOR INFORMATION

Corresponding Authors

Robin Lundström − *Department of Chemistry, Ångström Laboratory, Uppsala University, SE-751 21 Uppsala, Sweden;* orcid.org/0000-0001-9070-9264; Email: robin.lundstrom@kemi.uu.se

Erik J. Berg − *Department of Chemistry, Ångström Laboratory, Uppsala University, SE-751 21 Uppsala, Sweden;* orcid.org/0000-0001-5653-0383; Email: erik.berg@kemi.uu.se

https://doi.org/10.1021/acs.jpcc.4c00927
J. Phys. Chem. C 2024, 128, 8147−8153

Authors

Neeha Gogoi − *Department of Chemistry, Ångström Laboratory, Uppsala University, SE-751 21 Uppsala, Sweden;* orcid.org/0000-0002-0481-5544

Tim Melin − *Department of Chemistry, Ångström Laboratory, Uppsala University, SE-751 21 Uppsala, Sweden;* orcid.org/0000-0001-6691-6706

Complete contact information is available at: https://pubs.acs.org/10.1021/acs.jpcc.4c00927

Notes

The authors declare no competing financial interest.

■ ACKNOWLEDGMENTS

Knut and Alice Wallenberg (KAW) Foundation (Grant 2017.0204) and Stiftelsen för Strategisk Forskning (SSF, FFL18-0269) are thanked for financial support. StandUp for Energy is thanked for base funding.

■ REFERENCES

(1) Peled, E.; Menkin, S. Review—SEI: Past, Present and Future. *J. Electrochem. Soc.* **2017**, *164* (7), A1703−A1719.

(2) Spotte-Smith, E. W. C.; Kam, R. L.; Barter, D.; Xie, X.; Hou, T.; Dwaraknath, S.; Blau, S. M.; Persson, K. A. Toward a Mechanistic Model of Solid−Electrolyte Interphase Formation and Evolution in Lithium-Ion Batteries. *ACS Energy Lett.* **2022**, *7* (7), 1446−1453.

(3) Kim, S.; Kim, H. S.; Kim, B.; Kim, Y. J.; Jung, J. W.; Ryu, W. H. In Situ Gas Analysis by Differential Electrochemical Mass Spectrometry for Advanced Rechargeable Batteries: A Review. *Adv. Energy Mater.* **2023**, *13* (39), 1−33.

(4) Rowden, B.; Garcia-Araez, N. A Review of Gas Evolution in Lithium Ion Batteries. *Energy Rep.* **2020**, *6*, 10−18.

(5) Mogi, R.; Inaba, M.; Iriyama, Y.; Abe, T.; Ogumi, Z. Study on the Decomposition Mechanism of Alkyl Carbonate on Lithium Metal by Pyrolysis-Gas Chromatography-Mass Spectroscopy. *J. Power Sources* **2003**, *121*, 597−603, DOI: 10.1016/S0378-7753(03)00302-1.

(6) Kong, W.; Li, H.; Huang, X.; Chen, L. Gas Evolution Behaviors for Several Cathode Materials in Lithium-Ion Batteries. *J. Power Sources* **2005**, *142* (1−2), 285−291.

(7) Onuki, M.; Kinoshita, S.; Sakata, Y.; Yanagidate, M.; Otake, Y.; Ue, M.; Deguchi, M. Identification of the Source of Evolved Gas in Li-Ion Batteries Using [Sup 13]C-Labeled Solvents. *J. Electrochem. Soc.* **2008**, *155* (11), A794.

(8) Haregewoin, A. M.; Leggesse, E. G.; Jiang, J. C.; Wang, F. M.; Hwang, B. J.; Lin, S. D. Comparative Study on the Solid Electrolyte Interface Formation by the Reduction of Alkyl Carbonates in Lithium Ion Battery. *Electrochim. Acta* **2014**, *136*, 274−285.

(9) Aurbach, D.; Markovsky, B.; Shechter, A.; Ein-Eli, Y.; Cohen, H. A Comparative Study of Synthetic Graphite and Li Electrodes in Electrolyte Solutions Based on Ethylene Carbonate-Dimethyl Carbonate Mixtures. *J. Electrochem. Soc.* **1996**, *143* (12), 3809−3820.

(10) Seo, D. M.; Chalasani, D.; Parimalam, B. S.; Kadam, R.; Nie, M.; Lucht, B. L. Reduction Reactions of Carbonate Solvents for Lithium Ion Batteries. *Batteries* **2014**, *3*, A91−A94, DOI: 10.1149/2.0021409eel.

(11) Imhof, R.; Novák, P. In Situ Investigation of the Electrochemical Reduction of Carbonate Electrolyte Solutions at Graphite Electrodes. *J. Electrochem. Soc.* **1998**, *145* (4), 1081−1087.

(12) Edström, K.; Herstedt, M.; Abraham, D. P. A New Look at the Solid Electrolyte Interphase on Graphite Anodes in Li-Ion Batteries. *J. Power Sources* **2006**, *153* (2), 380−384.

(13) Verma, P.; Maire, P.; Novák, P. A Review of the Features and Analyses of the Solid Electrolyte Interphase in Li-Ion Batteries. *Electrochim. Acta* **2010**, *55* (22), 6332−6341.

(14) Yoshida, H.; Fukunaga, T.; Hazama, T.; Terasaki, M.; Mizutani, M.; Yamachi, M. Degradation Mechanism of Alkyl Carbonate Solvents Used in Lithium-Ion Cells during Initial Charging. *J. Power Sources* **1997**, *68* (2), 311−315.

(15) Xu, K. Electrolytes and Interphases in Li-Ion Batteries and Beyond. *Chem. Rev.* **2014**, *114* (23), 11503−11618.

(16) Ota, H.; Sakata, Y.; Inoue, A.; Yamaguchi, S. Analysis of Vinylene Carbonate Derived SEI Layers on Graphite Anode. *J. Electrochem. Soc.* **2004**, *151* (10), A1659.

(17) Buqa, H.; Würsig, A.; Vetter, J.; Spahr, M. E.; Krumeich, F.; Novák, P. SEI Film Formation on Highly Crystalline Graphitic Materials in Lithium-Ion Batteries. *J. Power Sources* **2006**, *153* (2), 385−390.

(18) Xiong, D.; Burns, J. C.; Smith, A. J.; Sinha, N.; Dahn, J. R. A High Precision Study of the Effect of Vinylene Carbonate (VC) Additive in Li/Graphite Cells. *J. Electrochem. Soc.* **2011**, *158* (12), A1431.

(19) Burns, J. C.; Sinha, N. N.; Coyle, D. J.; Jain, G.; VanElzen, C. M.; Lamanna, W. M.; Xiao, A.; Scott, E.; Gardner, J. P.; Dahn, J. R. The Impact of Varying the Concentration of Vinylene Carbonate Electrolyte Additive in Wound Li-Ion Cells. *J. Electrochem. Soc.* **2011**, *159* (2), A85−A90.

(20) Zhang, B.; Metzger, M.; Solchenbach, S.; Payne, M.; Meini, S.; Gasteiger, H. A.; Garsuch, A.; Lucht, B. L. Role of 1,3-Propane Sultone and Vinylene Carbonate in Solid Electrolyte Interface Formation and Gas Generation. *J. Phys. Chem. C* **2015**, *119* (21), 11337−11348.

(21) Kitz, P. G.; Lacey, M. J.; Novák, P.; Berg, E. J. Operando Investigation of the Solid Electrolyte Interphase Mechanical and Transport Properties Formed from Vinylene Carbonate and Fluoroethylene Carbonate. *J. Power Sources* **2020**, *477*, No. 228567, DOI: 10.1016/j.jpowsour.2020.228567.

(22) Nie, M.; Demeaux, J.; Young, B. T.; Heskett, D. R.; Chen, Y.; Bose, A.; Woicik, J. C.; Lucht, B. L. Effect of Vinylene Carbonate and Fluoroethylene Carbonate on SEI Formation on Graphitic Anodes in Li-Ion Batteries. *J. Electrochem. Soc.* **2015**, *162* (13), A7008−A7014.

(23) Grugeon, S.; Jankowski, P.; Cailleu, D.; Forestier, C.; Sannier, L.; Armand, M.; Johansson, P.; Laruelle, S. Towards a Better Understanding of Vinylene Carbonate Derived SEI-Layers by Synthesis of Reduction Compounds. *J. Power Sources* **2019**, *427*, 77−84, DOI: 10.1016/j.jpowsour.2019.04.061.

(24) Michan, A. L.; Parimalam, B. S.; Leskes, M.; Kerber, R. N.; Yoon, T.; Grey, C. P.; Lucht, B. L. Fluoroethylene Carbonate and Vinylene Carbonate Reduction: Understanding Lithium-Ion Battery Electrolyte Additives and Solid Electrolyte Interphase Formation. *Chem. Mater.* **2016**, *28* (22), 8149−8159.

(25) Schwenke, K. U.; Solchenbach, S.; Demeaux, J.; Lucht, B. L.; Gasteiger, H. A. The Impact of CO 2 Evolved from VC and FEC during Formation of Graphite Anodes in Lithium-Ion Batteries. *J. Electrochem. Soc.* **2019**, *166* (10), A2035−A2047.

(26) Forestier, C.; Grugeon, S.; Davoisne, C.; Lecocq, A.; Marlair, G.; Armand, M.; Sannier, L.; Laruelle, S. Graphite Electrode Thermal Behavior and Solid Electrolyte Interphase Investigations: Role of State-of-the-Art Binders, Carbonate Additives and Lithium Bis-(Fluorosulfonyl)Imide Salt. *J. Power Sources* **2016**, *330*, 186−194.

(27) El Ouatani, L.; Dedryvère, R.; Siret, C.; Biensan, P.; Reynaud, S.; Iratçabal, P.; Gonbeau, D. The Effect of Vinylene Carbonate Additive on Surface Film Formation on Both Electrodes in Li-Ion Batteries. *J. Electrochem. Soc.* **2009**, *156* (2), A103.

(28) Kubot, M.; Balke, L.; Scholz, J.; Wiemers-Meyer, S.; Karst, U.; Hayen, H.; Hur, H.; Winter, M.; Kasnatscheew, J.; Nowak, S. High-Voltage Instability of Vinylene Carbonate (VC): Impact of Formed Poly-VC on Interphases and Toxicity. *Adv. Sci.* **2023**, *11* (1), No. 2305282, DOI: 10.1002/advs.202305282.

(29) Lundström, R.; Gogoi, N.; Hou, X.; Berg, E. J. Competing Ethylene Carbonate Reactions on Carbon Electrode in Li-Ion Batteries. *J. Electrochem. Soc.* **2023**, *170* (4), No. 040516.

(30) Lundström, R.; Berg, E. J. Design and Validation of an Online Partial and Total Pressure Measurement System for Li-Ion Cells. *J. Power Sources* **2021**, *485*, No. 229347, DOI: 10.1016/j.jpowsour.2020.229347.

(31) Park, M. S.; Ma, S. B.; Lee, D. J.; Im, D.; Doo, S. G.; Yamamoto, O. A Highly Reversible Lithium Metal Anode. *Sci. Rep.* **2014**, *4*, No. 3815, DOI: 10.1038/srep03815.
(32) Han, J. G.; Kim, K.; Lee, Y.; Choi, N. S. Scavenging Materials to Stabilize LiPF 6 -Containing Carbonate-Based Electrolytes for Li-Ion Batteries. *Adv. Mater.* **2019**, *31* (20), No. 1804822, DOI: 10.1002/adma.201804822.
(33) Nagaoka, T.; Fukunaga, T.; Yoshino, T.; Watanabe, I.; Nakayama, T.; Okazaki, S. Uptake of Ions into Electrochemically Treated Glassy Carbon. *Anal. Chem.* **1988**, *60* (24), 2766−2769.
(34) Solchenbach, S.; Huang, X.; Pritzl, D.; Landesfeind, J.; Gasteiger, H. A. Monitoring SEI Formation on Graphite Electrodes in Lithium-Ion Cells by Impedance Spectroscopy. *J. Electrochem. Soc.* **2021**, *168* (11), No. 110503.
(35) Zhang, X.; Fan, C.; Xiao, P.; Han, S. Effect of Vinylene Carbonate on Electrochemical Performance and Surface Chemistry of Hard Carbon Electrodes in Lithium Ion Cells Operated at Different Temperatures. *Electrochim. Acta* **2016**, *222*, 221−231.
(36) Petibon, R.; Xia, J.; Burns, J. C.; Dahn, J. R. Study of the Consumption of Vinylene Carbonate in Li[Ni 0.33 Mn 0.33 Co 0.33] O 2 /Graphite Pouch Cells. *J. Electrochem. Soc.* **2014**, *161* (10), A1618−A1624.
(37) Metzger, M.; Strehle, B.; Solchenbach, S.; Gasteiger, H. A. Origin of H 2 Evolution in LIBs: H 2 O Reduction vs. Electrolyte Oxidation. *J. Electrochem. Soc.* **2016**, *163* (5), A798−A809.
(38) Bernhard, R.; Metzger, M.; Gasteiger, H. A. Gas Evolution at Graphite Anodes Depending on Electrolyte Water Content and SEI Quality Studied by On-Line Electrochemical Mass Spectrometry. *J. Electrochem. Soc.* **2015**, *162* (10), 1984−1989.

https://doi.org/10.1021/acs.jpcc.4c00927
J. Phys. Chem. C 2024, 128, 8147−8153